Elliptic flow: a brief review

Elliptic flow: a brief review

Raimond Snellings

Utrecht University, PO Box 80000, 3508 TA Utrecht, The Netherlands
E-mail: R.J.M.Snellings@uv.nl

Abstract. One of the fundamental questions in the field of subatomic physics is the question of what happens to matter at extreme densities and temperatures as may have existed in the first microseconds after the Big Bang and exists, perhaps, in the core of dense neutron stars. The aim of heavy-ion physics is to collide nuclei at very high energies and thereby create such a state of matter in the laboratory. The experimental program began in the 1990s with collisions made available at the Brookhaven Alternating Gradient Synchrotron (AGS) and the CERN Super Proton Synchrotron (SPS), and continued at the Brookhaven Relativistic Heavy-Ion Collider (RHIC) with the maximum center-of-mass energies of $\sqrt{s_{\mathrm{NN}}} = 4.75$, 17.2 and 200 GeV, respectively. Collisions of heavy ions at the unprecedented energy of 2.76 TeV recently became available at the LHC collider at CERN. In this review, I give a brief introduction to the physics of ultrarelativistic heavy-ion collisions and discuss the current status of elliptic flow measurements.

Contents

IOP Institute of Physics ⏺ DEUTSCHE PHYSIKALISCHE GESELLSCHAFT

1. Heavy-ion physics

According to our current understanding, the universe went through a series of phase transitions that mark the most important epochs of the expanding universe after the Big Bang. At 10^{-11} s and at a temperature of $T \sim 100\,\text{GeV}$ ($\sim 10^{15}\,\text{K}$), the electroweak phase, transition took place where most of the known elementary particles acquired their Higgs masses [1–3]. At 10^{-5} s and at a temperature of $\sim 200\,\text{MeV}$ ($\sim 10^{12}\,\text{K}$), the strong phase transition took place, where the quarks and gluons became confined into hadrons and where the approximate chiral symmetry was spontaneously broken [4].

Quantum chromodynamics (QCD) is the underlying theory of the strong force. Although its fundamental degrees of freedom (quarks and gluons) cannot be observed as free particles, the QCD Lagrangian is well established. One of the key features of QCD is the self-coupling of the gauge bosons (gluons), which cause the coupling constant to increase with decreasing momentum transfer. This running of the coupling constant gives rise to asymptotic freedom [5, 6] and confinement at large and small momentum transfers, respectively. At small momentum transfer, nonperturbative corrections, which are notoriously hard to calculate, become important. For this reason, two important nonperturbative properties of QCD, namely confinement and chiral symmetry breaking, are still poorly understood from first principles.

One of the fundamental questions in QCD phenomenology is the question of what the properties of matter are at extreme densities and temperatures, where the quarks and gluons are in a deconfined state, the so-called quark gluon plasma (QGP) [7]. Basic arguments [7] allow us to estimate the energy density $\epsilon \sim 1\,\text{GeV}\,\text{fm}^{-3}$ and temperature $T \sim 200\,\text{MeV}$ at which the strong phase transition takes place. These values imply that the transition occurs in a regime where the coupling constant is large so that we cannot rely anymore on perturbative QCD. A better understanding of the non-perturbative domain comes from lattice QCD, where the field equations are solved numerically on a discrete space–time grid. Lattice QCD provides quantitative information about the QCD phase transition and the equation of state (EoS) of the deconfined state. At extreme temperatures (large momenta), we expect that the quarks and gluons will be weakly interacting and that the QGP will behave as an ideal gas. For an ideal massless gas, the EoS is given by

$$P = \frac{1}{3}\epsilon, \qquad \epsilon = g\frac{\pi^2}{30}T^4, \tag{1}$$

where P is the pressure, ϵ the energy density, T the temperature and g the effective number of degrees of freedom. Each bosonic degree of freedom contributes 1 unit to g, whereas each fermionic degree of freedom contributes $\frac{7}{8}$. The value of g and 47.5 for a three-flavor QGP, which is an order of magnitude larger than that for a pion gas, namely $g \sim 3$.

Figure 1 shows the temperature dependence of the energy density as calculated from lattice QCD [8]. It is seen that the energy density changes rapidly around $T \sim 190\,\text{MeV}$, which is due to the rapid increase in the effective degrees of freedom (lattice calculations show that the transition is a crossover). Also shown in figure 1 is the pressure, which changes slowly compared with the rapid increase in the energy density around $T = 190\,\text{MeV}$. It follows that the speed of sound, $c_s = \sqrt{\partial P/\partial \epsilon}$, is reduced during the strong phase transition. At high temperature, the energy density reaches a significant fraction (~ 0.9) of the ideal massless gas limit (Stefan–Boltzmann limit).

Relativistic heavy-ion collisions are a unique tool to create and study hot QCD matter and its phase transition under controlled conditions [7], [9–13]. As in the early universe, the
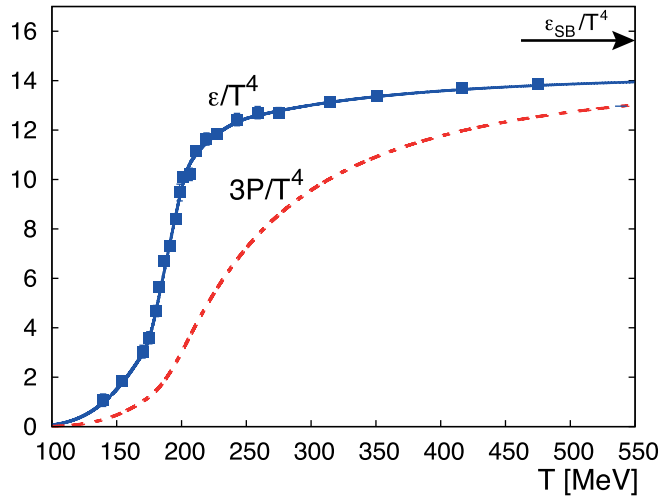
Figure 1. Energy density ϵ/T^4 (full curve) and pressure $3P/T^4$ (dashed curve) as a function of temperature T from lattice calculations [8]. The arrow indicates the Stefan–Boltzmann limit of the energy density.

hot and dense system created in a heavy-ion collision will expand and cool down. During this evolution, the system probes a range of energy densities and temperatures and possibly different phases. Provided that the quarks and gluons undergo multiple interactions, the system will thermalize and form the QGP, which subsequently undergoes a collective expansion and eventually becomes so dilute that it hadronizes. This collective expansion is called flow.

Flow is an observable that provides experimental information about the equation of state and the transport properties of the created QGP. The azimuthal anisotropy in particle production is the clearest experimental signature of collective flow in heavy-ion collisions [14–18]. This so-called anisotropic flow is caused by the initial asymmetries in the geometry of the system produced in a non-central collision. The second Fourier coefficient of the azimuthal asymmetry is called elliptic flow. In this paper, I will describe the relation between elliptic flow and the geometry of the collision (sections 2 and 3), the sensitivity of elliptic flow to the EoS and transport properties (section 3) and the techniques used to measure elliptic flow from the data (section 4). In section 5, I will review the elliptic flow measurements at the LHC and at lower energies, together with the current theoretical understanding of these results.

2. Event characterization

Heavy ions are extended objects and the system created in a head-on collision is different from that in a peripheral collision. To study the properties of the created system, collisions are therefore categorized by their centrality. Theoretically, the centrality is defined by the impact parameter **b** (see figure 2), which, however, cannot be directly observed.

Experimentally, the collision centrality can be inferred from the measured particle multiplicities, given the assumption that the multiplicity is a monotonic function of **b**. The centrality is then characterized by the fraction, $\pi b^2/\pi(2R_A)^2$, of the geometrical cross-section, with R_A being the nuclear radius (see figure 3(a)).
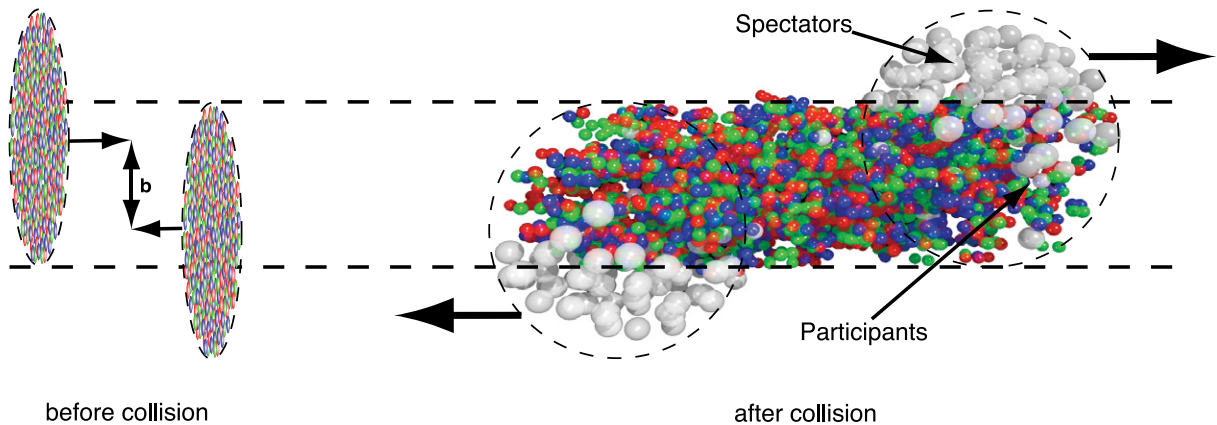
Spectators

Participants

before collision   after collision

Figure 2. Left: the two heavy ions before the collision with the impact parameter **b**. Right: the spectators remain unaffected while in the participant zone, particle production takes place.
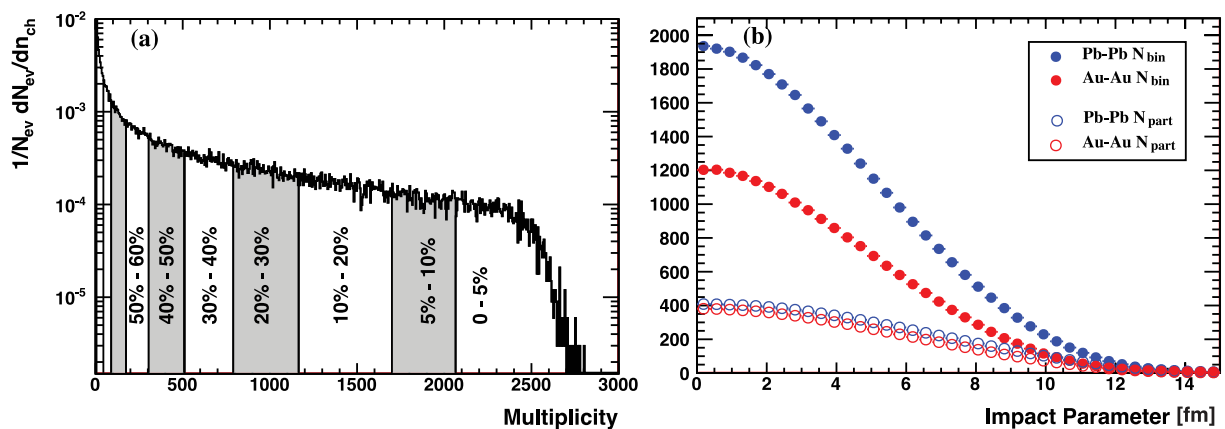

Figure 3. (a) Charged particle distribution from Pb–Pb collisions at $\sqrt{s_{NN}} = 2.76$ TeV measured with ALICE, showing a classification in centrality percentiles (from [20]). (b) The number of participating nucleons N_{part} and binary collisions N_{bin} versus the impact parameter for Pb–Pb and Au–Au collisions at $\sqrt{s_{NN}} = 2.76$ and 0.2 TeV, respectively.

Instead of by the impact parameter, the centrality is also often characterized by the number of participating nucleons (nucleons that undergo at least one inelastic collision) or by the number of equivalent binary collisions. Phenomenologically, it is found that the total particle production scales with the number of participating nucleons, whereas hard processes scale with the number of binary collisions. These measures can be related to the impact parameter **b** using a realistic description of the nuclear geometry in a Glauber calculation [19], as shown in figure 3(b). This figure also shows that Pb–Pb collisions at $\sqrt{s_{NN}} = 2.76$ TeV and Au–Au collisions at $\sqrt{s_{NN}} = 0.2$ TeV have a similar distribution of participating nucleons. The number of binary collisions increases from Au–Au to Pb–Pb by about 50%, because the nucleon–nucleon inelastic cross-section increases by about that amount at the respective center-of-mass energies of 0.2 and 2.76 TeV.
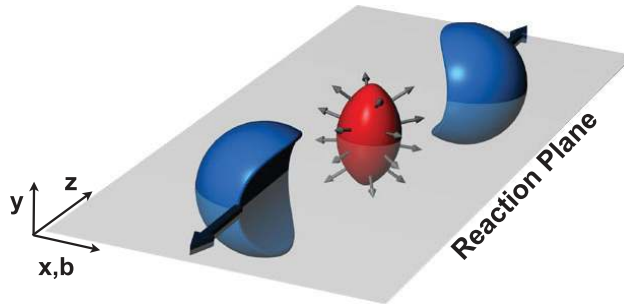
Figure 4. Almond-shaped interaction volume after a non-central collision of two nuclei. The spatial anisotropy with respect to the x–z plane (reaction plane) translates into a momentum anisotropy of the produced particles (anisotropic flow).

3. Anisotropic flow

Flow signals the presence of multiple interactions between the constituents of the medium created in the collision. An increasing number of interactions usually leads to a larger magnitude of flow and brings the system closer to thermalization. The magnitude of the flow is therefore a detailed probe of the level of thermalization.

The theoretical tools for describing flow are hydrodynamics or microscopic transport (cascade) models. In the transport models, flow depends on the opacity of the medium, be it partonic or hadronic. Hydrodynamics become applicable when the mean free path of the particles is much smaller than the system size, and allow for a description of the system in terms of macroscopic quantities. This gives a handle on the equation of state of the flowing matter and, in particular, on the value of the sound velocity c_s.

Experimentally, the most direct evidence of flow comes from the observation of anisotropic flow, which is the anisotropy in particle momentum distributions correlated to the reaction plane. The reaction plane is defined by the impact parameter and the beam direction z (see figure 4). A convenient way of characterizing the various patterns of anisotropic flow is to use a Fourier expansion of the invariant triple differential distributions,

$$E\frac{\mathrm{d}^3 N}{\mathrm{d}^3 \mathbf{p}} = \frac{1}{2\pi}\frac{\mathrm{d}^2 N}{p_t \mathrm{d}p_t \mathrm{d}y}\left(1 + 2\sum_{n=1}^{\infty} v_n \cos[n(\varphi - \Psi_{\mathrm{RP}})]\right), \tag{2}$$

where E is the energy of the particle, p the momentum, p_t the transverse momentum, φ the azimuthal angle, y the rapidity and Ψ_{RP} the reaction plane angle. The sine terms in such an expansion vanish because of the reflection symmetry with respect to the reaction plane. The Fourier coefficients are p_t and y dependent and are given by

$$v_n(p_t, y) = \langle \cos[n(\varphi - \Psi_{\mathrm{RP}})] \rangle, \tag{3}$$

where the angular brackets denote an average over the particles, summed over all events, in the (p_t, y) bin under study. In this Fourier decomposition, the coefficients v_1 and v_2 are known as directed flow and elliptic flow, respectively.

The evolution of the almond-shaped interaction volume is shown in figure 5. The contours indicate the energy density profile and the plots from left to right show how the system evolves
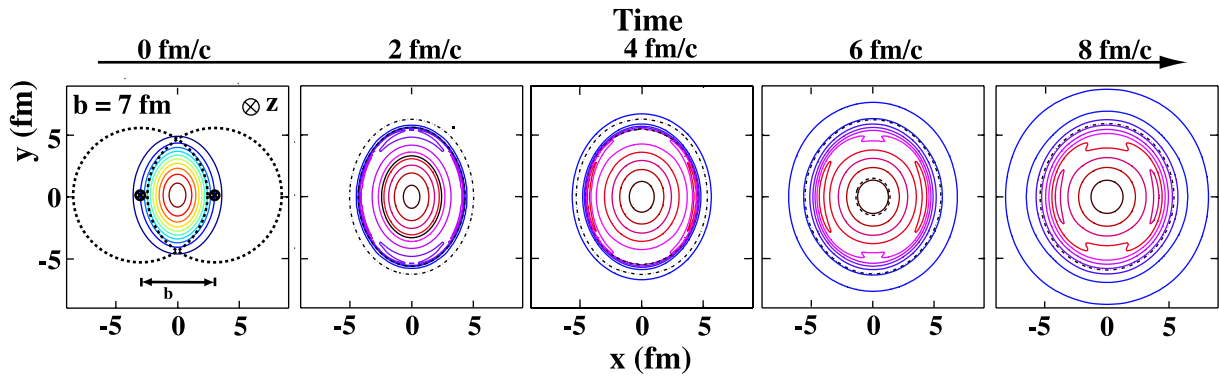
Figure 5. The created initial transverse energy density profile and its time dependence in coordinate space for a non-central heavy-ion collision [21]. The z-axis is along the colliding beams and the x-axis is defined by the impact parameter.
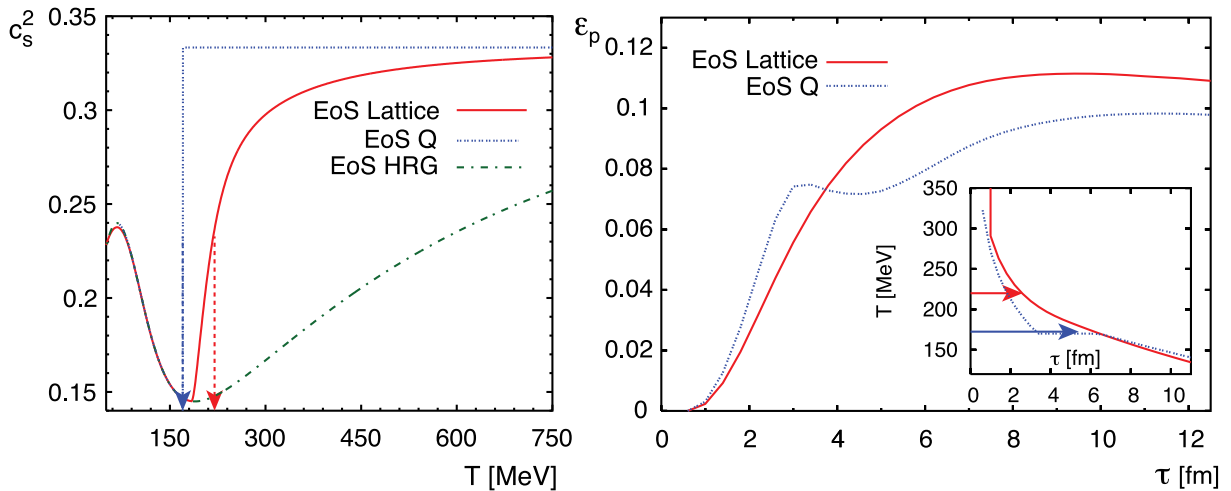

Figure 6. (a) The velocity of sound squared versus temperature for three equations of state [22]. (b) The anisotropy in momentum space for the two equations of state used in hydrodynamic calculations [22].

from an almond-shaped transverse overlap region into an almost symmetric system. During this expansion, governed by the velocity of sound, the created hot and dense system cools down.

Figure 6(a) shows the velocity of sound versus temperature for three different equations of state [22]. The dash-dotted line is the hadron resonance gas EoS, the red full line is a parameterization of the EoS that matches recent lattice calculations and the blue dashed line is an EoS that incorporates a first-order phase transition. The arrows indicate the corresponding transition temperatures for the lattice-inspired EoS and the EoS with a first-order phase transition. The temperature dependence of the sound velocity clearly differs significantly across the different equations of state. Because the expansion of the system and the buildup of collective motion depend on the velocity of sound, it is expected that this difference will have a clear signature in the flow. The buildup of the flow for two different EoS is shown in figure 6(b). Due to the stronger expansion in the reaction plane, the initial almond-shaped anisotropy in
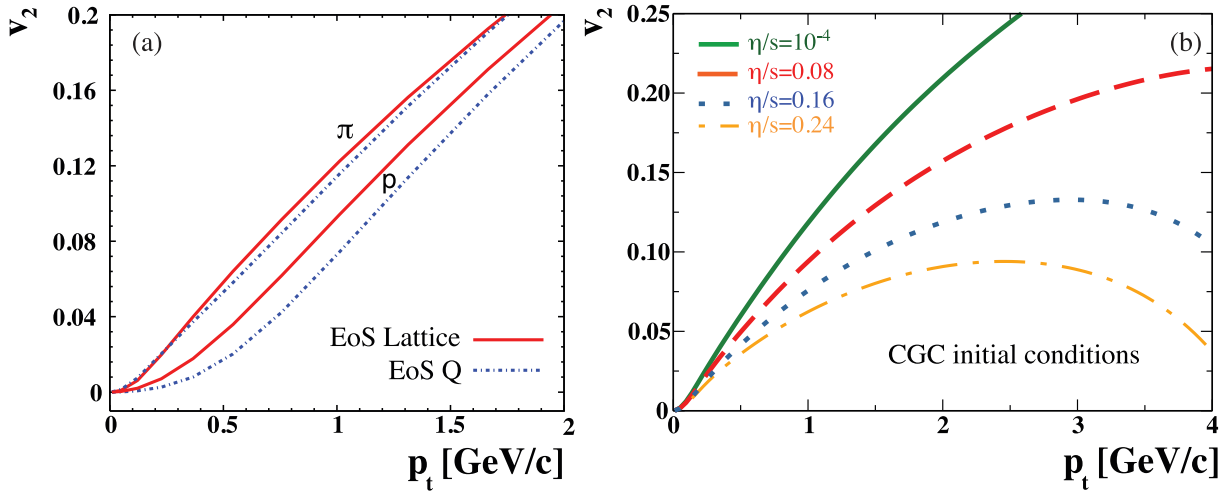
Figure 7. (a) The EoS dependence of $v_2(p_t)$ in the case of pions and protons [22]. The full lines are for the lattice-inspired EoS and the dashed lines are for an EoS that incorporates a first-order phase transition. (b) The dependence of $v_2(p_t)$ on η/s in the case of charged particles [24].

coordinate space vanishes, as was shown in figure 5, while the momentum space distribution changes in the opposite direction from being approximately azimuthally symmetric to having a preferred direction in the reaction plane. The asymmetry in momentum space can be quantified by

$$\varepsilon_p = \frac{\langle T_{xx} - T_{yy} \rangle}{\langle T_{xx} + T_{yy} \rangle}, \tag{4}$$

where T_{xx} and T_{yy} are the diagonal transverse components of the energy momentum tensor and the brackets denote an averaging over the transverse plane. Figure 6(b) shows that ε_p versus time starts at zero, after which the anisotropy rapidly develops, and is indeed dependent on the EoS.

Although ε_p is not a direct observable, the observed EoS dependence of ε_p versus time is reflected in the experimental observable v_2, in particular when plotted as a function of transverse momentum and particle mass. Figure 7(a) shows p_t-differential elliptic flow for pions and protons after the transverse momentum spectra have been constrained. A clear mass dependence of v_2 at low transverse momentum is observed in the case of both equations of state. The figure also shows clearly that the pion v_2 does not differ much between the lattice EoS and EoS Q. On the other hand, the v_2 of protons does change significantly because heavier particles are more sensitive to a change in collective motion. Therefore, measurements of $v_2(p_t)$ for various particle species provide an excellent constraint on the EoS in ideal hydrodynamics.

More recently, it was realized that small deviations from the ideal hydrodynamics, in particular, viscous corrections, already modify significantly the buildup of the elliptic flow [23]. The shear viscosity determines how good a fluid is[1]; however, for relativistic fluids, the more useful quantity is the shear viscosity to entropy ratio η/s. Known good fluids in nature have an η/s of order $\hbar/k_B$. In a strongly coupled $\mathcal{N} = 4$ supersymmetric Yang–Mills theory with a large

---

[1] A good fluid has a low viscosity and does not convert much kinetic energy of the flow into heat.
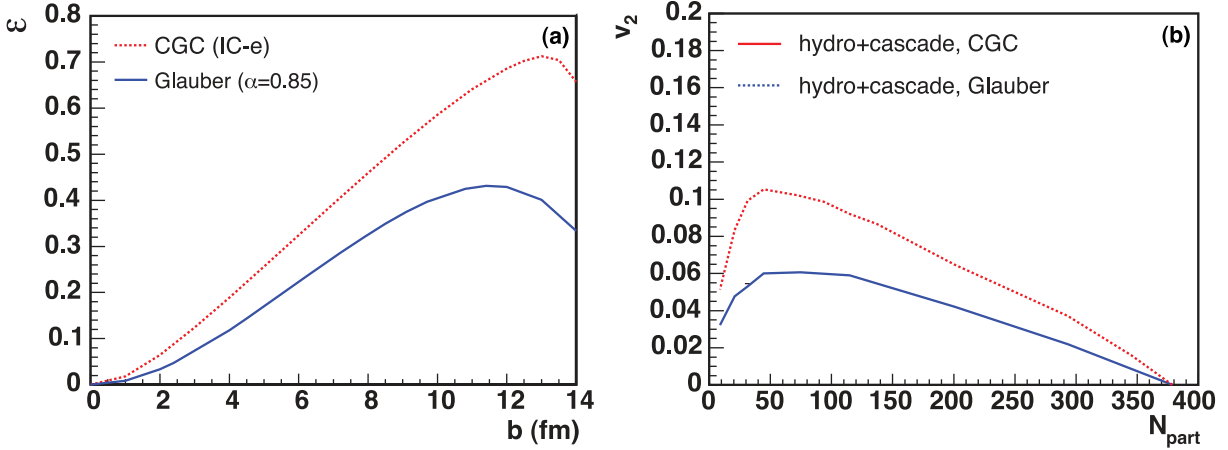
Figure 8. (a) The eccentricity ε values calculated using a CGC model and a Glauber model [28]. (b) The v_2 obtained using the CGC or Glauber initial eccentricity [28].

number of colors ('t Hooft limit), η/s can be calculated using a gauge gravity duality [25],

$$\frac{\eta}{s} = \frac{\hbar}{4\pi k_{\mathrm{B}}}.$$

Kovtun *et al* [25] conjectured, using the AdS/CFT correspondence, that this implies that all fluids have $\eta/s \geqslant \hbar/4\pi k_{\mathrm{B}}$ (the KSS bound). We therefore call a fluid with $\eta/s = 1/4\pi$ (in natural units) a perfect fluid. The KSS bound raises the interesting question of how fundamental this value is in nature and whether the QGP behaves like an almost perfect fluid. It is argued that the transition from hadrons to quarks and gluons occurs in the vicinity of the minimum in η/s, just as is the case for the phase transitions in helium, nitrogen and water. An experimental measurement of the minimal value of η/s would thus pinpoint the location of the transition [26, 27].

Experimentally, we might get an answer to the magnitude of η/s by measuring v_2, as shown in figure 7(b). The full line is close to ideal hydrodynamics ($\eta/s \sim 0$), while the other three lines correspond to those η/s values that are up to three times the KSS bound. Different magnitudes of η/s clearly lead to a significantly different magnitude of v_2 and change its p_{t} dependence. However, the magnitude and p_{t} dependence of v_2 depend not only on η/s but also on the EoS, as we have seen.

The magnitude of v_2 is not only dependent on the medium properties of interest but also proportional to the initial spatial anisotropy of the collision region. This spatial anisotropy can be characterized by eccentricity, which is defined by

$$\varepsilon = \frac{\langle y^2 - x^2 \rangle}{\langle y^2 + x^2 \rangle}, \tag{5}$$

where x and y are the positions of the participating nucleons in the transverse plane and the brackets denote an average that traditionally was taken over the number of participants. Recent calculations have shown that the eccentricity obtained in different descriptions, in particular by comparing a Glauber with a color glass condensate (CGC) description, indicates that ε varies by almost 25% at a given impact parameter [28] (see figure 8(a)). The elliptic flow obtained using
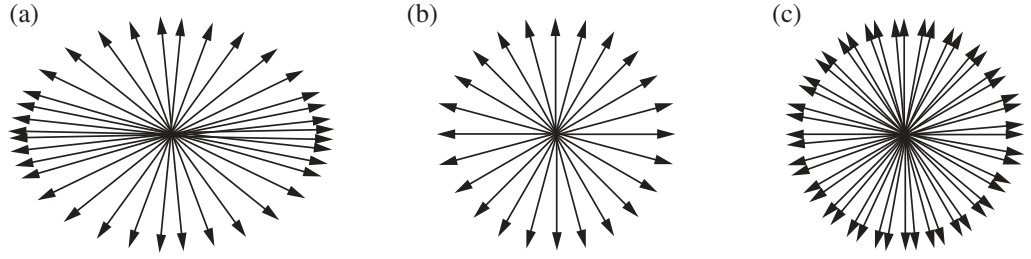
Figure 9. Examples of particle distributions in the transverse plane, where for (a) $v_2 > 0$, $v_2\{2\} > 0$, (b) $v_2 = 0$, $v_2\{2\} = 0$ and (c) $v_2 = 0$, $v_2\{2\} > 0$.

these different initial eccentricities is shown in figure 8(b). As expected, the different magnitudes of the eccentricity propagate to the magnitude of the elliptic flow. Because currently we cannot measure the eccentricity independently, this leads to a large uncertainty in the experimental determination of η/s.

   To summarize, we have seen that the elliptic flow depends not only on fundamental properties of the created matter, in particular the sound velocity and the shear viscosity, but also on the initial spatial eccentricity. Detailed measurements of elliptic flow as a function of transverse momentum, particle mass and collision centrality provide an experimental handle on these properties. In the next section, before we discuss the measurements, we first explain how we estimate the anisotropic flow experimentally.

4. Elliptic flow: analysis methods

Because the reaction plane angle is not a direct observable, the elliptic flow equation (3) cannot be measured directly and so it is usually estimated using azimuthal correlations between the observed particles. Two-particle azimuthal correlations, for example, can be written as

$$
\begin{aligned}
\langle\langle e^{i2(\varphi_1-\varphi_2)}\rangle\rangle &= \langle\langle e^{i2(\varphi_1-\Psi_{RP}-(\varphi_2-\Psi_{RP}))}\rangle\rangle, \\
&= \langle\langle e^{i2(\varphi_1-\Psi_{RP})}\rangle\langle e^{-i2(\varphi_2-\Psi_{RP})}\rangle + \delta_2\rangle, \\
&= \langle v_2^2 + \delta_2\rangle,
\end{aligned}
\tag{6}
$$

where the double brackets denote an average over all particles within an event, followed by averaging over all events. In equation (6), we have factorized the azimuthal correlation between the particles in a common correlation with the reaction plane (elliptic flow v_2) and a correlation independent of the reaction plane (non-flow δ_2). Here, we have assumed that the correlation between v_2 and δ_2 is negligible. If δ_2 is small, equation (6) can be used to measure $\langle v_2^2 \rangle$, but in general the non-flow contribution is not negligible.

   In figure 9, we illustrate two-particle non-flow contributions as follows. In figure 9(a), an anisotropic distribution is shown for which both $v_2 = \langle\cos 2\phi\rangle$ and the two-particle correlation $v_2\{2\} = \sqrt{\langle\cos 2(\phi_1 - \phi_2)\rangle}$ are positive. Figure 9(b) shows a symmetric distribution for which $v_2 = 0$ and also $v_2\{2\} = 0$. Figure 9(c) shows two symmetric distributions rotated with respect to each other, which give $v_2 = 0$ while $v_2\{2\}$ is non-zero. This illustrates how non-flow contributions from sources such as resonance decays or jets can contribute to v_2 measured from two-particle correlations.

IOP Institute of Physics **①** DEUTSCHE PHYSIKALISCHE GESELLSCHAFT

The collective nature of elliptic flow can be exploited to suppress non-flow contributions [29, 30]. This is done using so-called cumulants, which are genuine multi-particle correlations. For instance, the two-particle cumulant $c_2\{2\}$ and the four-particle cumulants $c_2\{4\}$ are defined as

$$c_2\{2\} \equiv \langle\langle e^{i2(\varphi_1 - \varphi_2)}\rangle\rangle = \langle v_2^2 + \delta_2\rangle. \tag{7}$$

$$\begin{aligned}
c_2\{4\} &\equiv \langle\langle e^{i2(\varphi_1 + \varphi_2 - \varphi_3 - \varphi_4)}\rangle\rangle - 2\langle\langle e^{i2(\varphi_1 - \varphi_2)}\rangle\rangle^2, \\
&= \langle v_2^4 + \delta_4 + 4v_2^2\delta_2 + 2\delta_2^2\rangle - 2\langle v_2^2 + \delta_2\rangle^2, \\
&= \langle -v_2^4 + \delta_4\rangle.
\end{aligned} \tag{8}$$

From the combinatorics, it is easy to show that $\delta_2 \propto 1/M_c$ and $\delta_4 \propto 1/M_c^3$, where M_c is the number of independent particle clusters. Therefore, $v_2\{2\}$ is a good estimate only if $v_2 \gg 1/\sqrt{M_c}$, whereas $v_2\{4\}$ is already a good estimate of v_2 if $v_2 \gg 1/M_c^{3/4}$; for $c_2\{\infty\}$ this argument leads to $v_2 \gg 1/M_c$. This shows that for a typical Pb–Pb collision at the LHC with $M_c = 500$ the possible non-flow contribution can be reduced by more than an order of magnitude using higher-order cumulants. One of the problems in using multi-particle correlations is the computing power needed to go over all possible particle multiplets. To avoid this problem, multi-particle correlations in heavy-ion collision are calculated from generating functions with numerical interpolations [29] or, as was shown more recently, from an exact solution [31].

The last equality in equation (8) follows from the assumption that v_2 and δ_2 are uncorrelated and also that $\langle\delta_2^2\rangle = \langle\delta_2\rangle^2$ and $\langle v_2^4\rangle = \langle v_2^2\rangle^2$. In other words, we have neglected the event-by-event fluctuations in v_2 and δ_2. The effect of the fluctuations on v_2 estimates can be obtained from

$$\langle v_2^2\rangle = \langle v_2\rangle^2 + \sigma^2, \qquad \langle v_2^4\rangle = \langle v_2\rangle^4 + 6\sigma^2\langle v_2\rangle^2, \qquad \langle v_2^6\rangle = \langle v_2\rangle^6 + 15\sigma^2\langle v_2\rangle^4. \tag{9}$$

Neglecting the non-flow terms, we have the following expressions for the cumulants,

$$v_2\{2\} = \sqrt{\langle v_2^2\rangle}, \qquad v_2\{4\} = \sqrt[4]{2\langle v_2^2\rangle^2 - \langle v_2^4\rangle}, \qquad v_2\{6\} = \sqrt[6]{\tfrac{1}{4}\left(\langle v_2^6\rangle - 9\langle v_2^2\rangle\langle v_2^4\rangle + 12\langle v_2^2\rangle^3\right)}. \tag{10}$$

Here we have introduced the notation $v_2\{n\}$ as the flow estimate from the cumulant $c_2\{n\}$. Assuming that $\sigma \ll \langle v\rangle$, we obtain from equations (9) and (10), up to order σ^2,

$$v_2\{2\} = \langle v_2\rangle + \frac{1}{2}\frac{\sigma^2}{\langle v_2\rangle}, \qquad v_2\{4\} = \langle v_2\rangle - \frac{1}{2}\frac{\sigma^2}{\langle v_2\rangle}, \qquad v_2\{6\} = \langle v_2\rangle - \frac{1}{2}\frac{\sigma^2}{\langle v_2\rangle}. \tag{11}$$

From equations (7) and (11), it is clear that the difference between $v_2\{2\}$ and $v_2\{4\}$ is sensitive to non-flow and fluctuations.

Flow fluctuations have become an important part of elliptic flow studies [32–42]. It is believed that such fluctuations originate mostly from fluctuations in the initial collision geometry. This is illustrated in figure 10, which shows participants that are randomly distributed in the overlap region. This collection of participants defines a participant plane Ψ_{PP} [33], which fluctuates, for each event, around the reaction plane Ψ_{RP}. These fluctuations can be estimated from calculations in, for instance, a Glauber model.

Figure 11(a) shows the eccentricities equation (5) calculated in a Glauber model. Here, $\varepsilon\{RP\}$ denotes the eccentricity in the reaction plane, ε is the participant eccentricity, and $\varepsilon\{2\}$ and $\varepsilon\{4\}$ are the participant eccentricities calculated using the cumulants, analogous to the
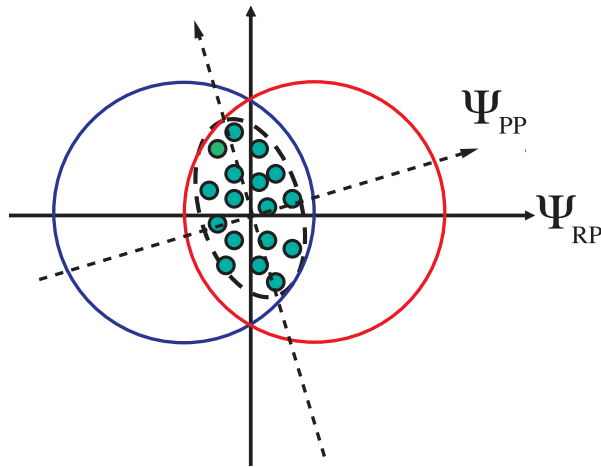
Figure 10. Transverse view of a heavy-ion collision with the reaction plane Ψ_{RP} oriented along the x-axis. Indicated are the participants in the overlap region that randomly define a participant plane Ψ_{PP} for each collision.
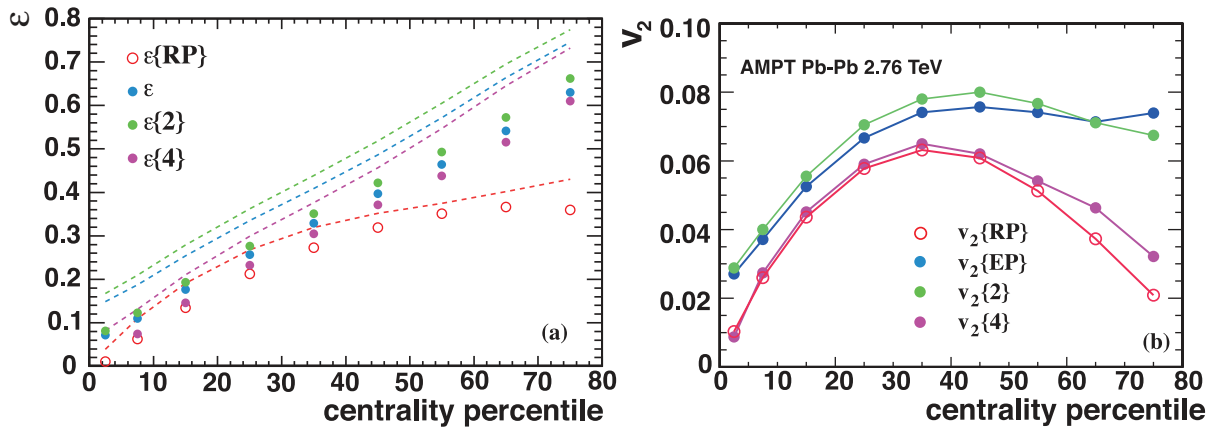

Figure 11. (a) The eccentricities from a Glauber calculation for participating nucleons (the solid and open markers) and binary collisions (the dashed lines). (b) Various v_2 estimates compared to the reaction plane value, $v_2\{RP\}$.

definitions in equation (10) [32]. In figure 11(a), the eccentricities are calculated using as a weight the participating nucleons (open and solid markers) or as a weight binary collisions (dashed lines). The figure clearly shows that in both cases, ε is in between $\varepsilon\{2\}$ and $\varepsilon\{4\}$, as is expected from equation (11). The figure also shows that $\varepsilon\{4\}$ is close to $\varepsilon\{RP\}$ in the 0–40% centrality range [40, 41]. In figure 11(b), we show a transport model calculation of v_2 in the AMPT model [43]. In this model, the true reaction plane is known so that we can compare the different v_2 estimates with the value in the reaction plane. The AMPT model uses a Glauber model for the initial conditions and we can therefore compare these estimates with figure 11(a) (the dashed lines). The agreement between $v_2\{4\}$ and $v_2\{RP\}$ holds for most of the centrality range, whereas for the eccentricities in the Glauber model, a large difference is observed in the case of the more peripheral collisions [42].
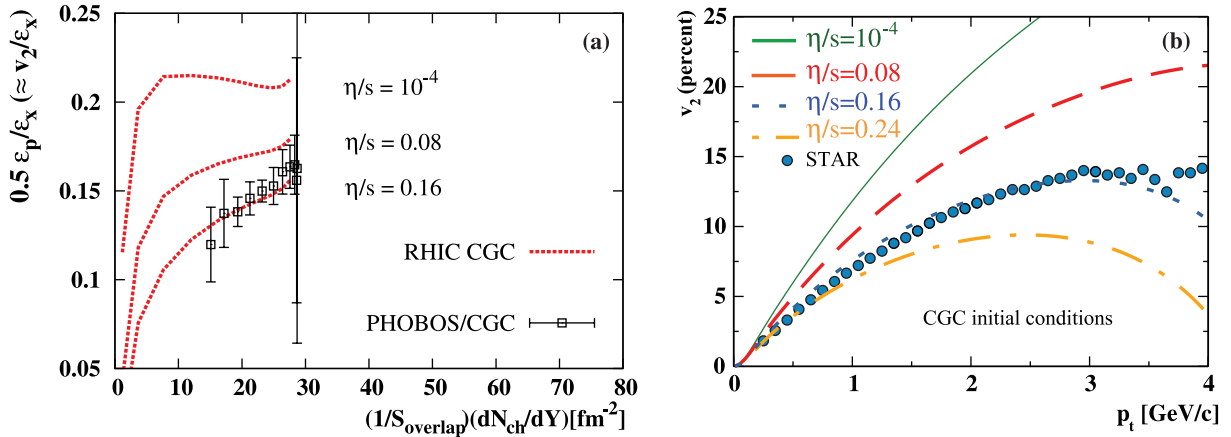
Figure 12. (a) The centrality dependence of $v_2\{2\}$ compared to viscous hydrodynamic model calculations [24]. (b) The transverse momentum dependence of v_2 compared to the same viscous hydrodynamic calculations [24].

5. Elliptic flow measurements

5.1. The perfect liquid

The large elliptic flow observed at the Relativistic Heavy-Ion Collider (RHIC) provides compelling evidence for strongly interacting matter that appears to behave like an almost perfect liquid [44, 45]. To quantify the agreement with an almost perfect fluid, the significant viscous corrections need to be calculated. Based on different model assumptions, the ratio η/s has been estimated at $\sqrt{s_{NN}} = 200\,\text{GeV}$ and is found to be less than five times the KSS bound [18], [46–49].

In figure 12, we show the centrality and transverse momentum dependence of v_2 compared with viscous hydrodynamic calculations [24] with different values of η/s. Using an eccentricity from a CGC-inspired calculation, it is seen that both the centrality and transverse momentum dependence are well described with an η/s that is two times the KSS bound. These calculations are performed on the assumption that the value of η/s is constant during the entire evolution. The value used in these calculations should be considered as an effective average of η/s, because we know from other fluids that η/s depends on temperature. In addition, we also know that part of the elliptic flow originates from the hadronic phase. Therefore, a knowledge of the temperature dependence *and* a knowledge of the relative contributions from the partonic and hadronic phases are required in order to quantify η/s of the partonic fluid.

Not only the v_2 of charged particles but also that of the identified particles at RHIC are described in the framework of viscous hydrodynamics at low p_t. Figure 13 shows the measured pion and proton elliptic flow measured by STAR compared with VISHNU [50] model calculations. The VISHNU model is a hybrid model that uses viscous hydrodynamics for the initial stage, followed by a hadron cascade afterburner. In the initial viscous hydrodynamic stage, η/s is temperature independent. The η/s magnitudes required to describe the pion and proton elliptic flow data are found to be one or two times the KSS bound for a Glauber or CGC eccentricity, respectively. This is in agreement with the magnitude of η/s required for describing charged particle v_2.
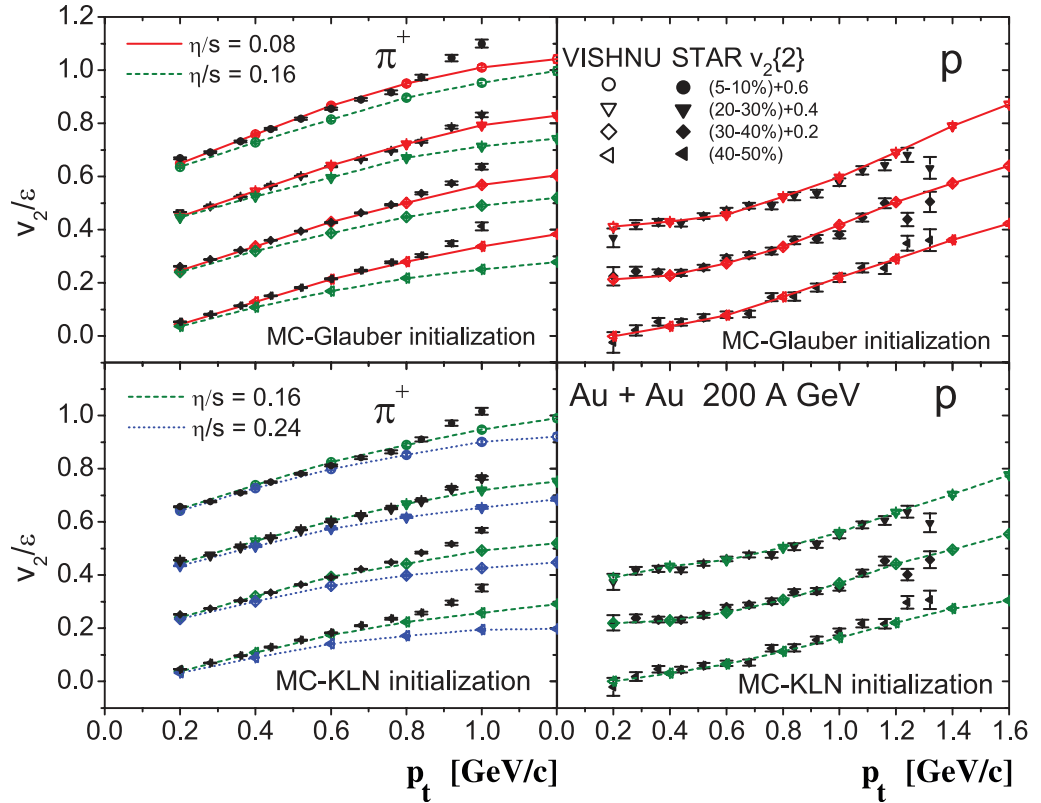
Figure 13. The $v_2(p_t)$ for pions and protons measured by STAR compared with model calculations with different eccentricities and η/s [50].

While the description of v_2 measurements is encouraging, it is important to realize that there are still large uncertainties in (i) the initial eccentricity, (ii) the relative contributions from the hadronic and partonic phases and (iii) the temperature dependence of η/s. Elliptic flow measurements at the LHC, with a higher center-of-mass energy, will constrain these uncertainties and will eventually provide a decisive test to identify which of the currently successful model descriptions is the more appropriate.

5.2. Energy dependence

Lead–lead collisions at the LHC are expected to produce a system that is hotter and has a longer-lived partonic phase than does the system created in Au–Au collisions at RHIC energies. As a consequence, the hadronic contribution to the elliptic flow decreases, which reduces the uncertainty in the determination of η/s in the partonic fluid. Because η/s is expected to depend on temperature in both the partonic and hadronic systems, it was not clear whether the elliptic flow would increase or decrease in going from RHIC to LHC energies. Hydrodynamic models [51–53] and hybrid models [54, 55] that successfully describe flow at RHIC predicted an increase of $\sim$10–30% in v_2.

Figure 14(a) shows the measured integrated elliptic flow at the LHC in one centrality bin, compared with the results from lower energies. It shows that there is a continuous increase in
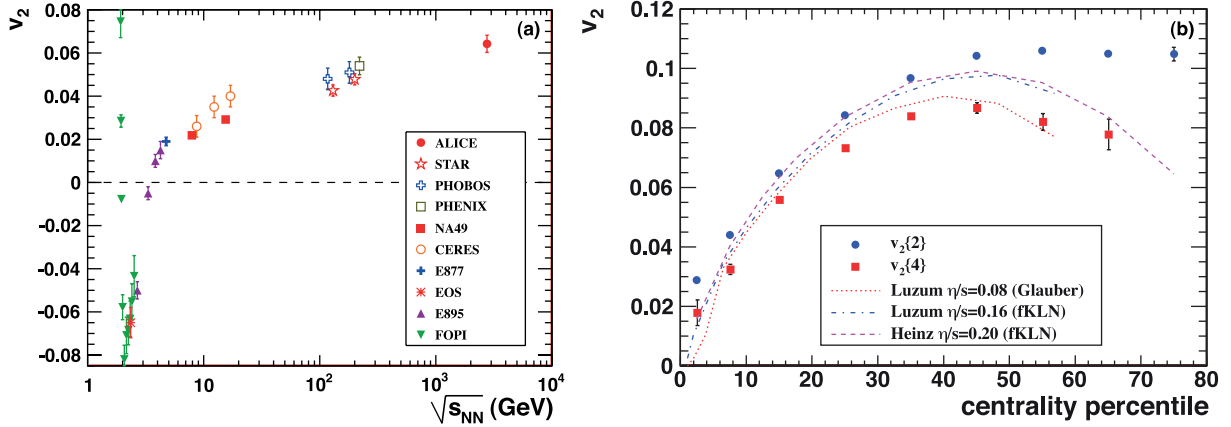
Figure 14. (a) Integrated elliptic flow at 2.76 TeV in the 20–30% centrality class compared with results from lower energies taken at similar centralities (from [20]). (b) Elliptic flow as a function of event centrality, for the two- (full circles) and four-particle (full squares) cumulant methods compared with viscous hydrodynamic calculations (dashed lines) [20, 56, 57].

the elliptic flow from RHIC to LHC energies. In comparison to the elliptic flow measurements in Au–Au collisions at $\sqrt{s_{NN}} = 200$ GeV, v_2 increases by about 30% at $\sqrt{s_{NN}} = 2.76$ TeV.

Figure 14(b) shows the v_2 for different centralities measured by ALICE with the two- and four-particle cumulant method. The difference between the two- and four-particle flow estimates for the more central collisions (<40%) is expected to be dominated by event-by-event flow fluctuations (see equation (11)). For the more peripheral collisions, the two-particle cumulant is likely biased by non-flow. We already mentioned that $v_2\{4\}$ yields estimates of the elliptic flow in the reaction plane, which can thus be compared to model predictions of $v_2\{RP\}$. The curves in figure 14(b) show $v_2\{RP\}$ from hydrodynamic model calculations for $\sqrt{s_{NN}} = 2.76$ TeV, with initial eccentricities and magnitudes of η/s, which described the RHIC data. It is seen that in hydrodynamic calculations, the observed increase in v_2 from RHIC to LHC energies is within expectations. Detailed comparisons, however, have to wait till measurements of identified particle spectra and identified particle elliptic flow become available. It will then be important to see if one still obtains a quantitative description of the data in viscous hydrodynamics and what the required magnitude of η/s will then be.

In addition to comparisons with detailed dynamic model calculations, we might also learn something from what happens to the several simple scaling properties observed at lower energies. For instance, it was shown that the integrated elliptic flow depends linearly on the pseudorapidity η, measured with respect to the beam rapidity y_{beam} [58], as shown in figure 15(a). Based on this scaling behavior, a phenomenological extrapolation [59] from RHIC to LHC was made (dashed line in figure 15(a)) that predicts an increase in v_2 of ∼50%, larger than the predictions from most other models. PHOBOS measured v_2 down to $p_t = 0$ using the eventplane method, which at RHIC is similar to measuring $v_2\{2\}$. The measurements at $\eta = 0$ for the LHC are below the triangular extrapolation. However, the elliptic flow as a function of pseudorapidity measured by ALICE at $|\eta| < 0.8$ (mesh in figure 15(a)) is constant within uncertainties. If one takes into account that the $v_2(\eta)$ does saturate, like the multiplicity, at each energy around midrapidity, then the longitudinal scaling might hold up to LHC energies.
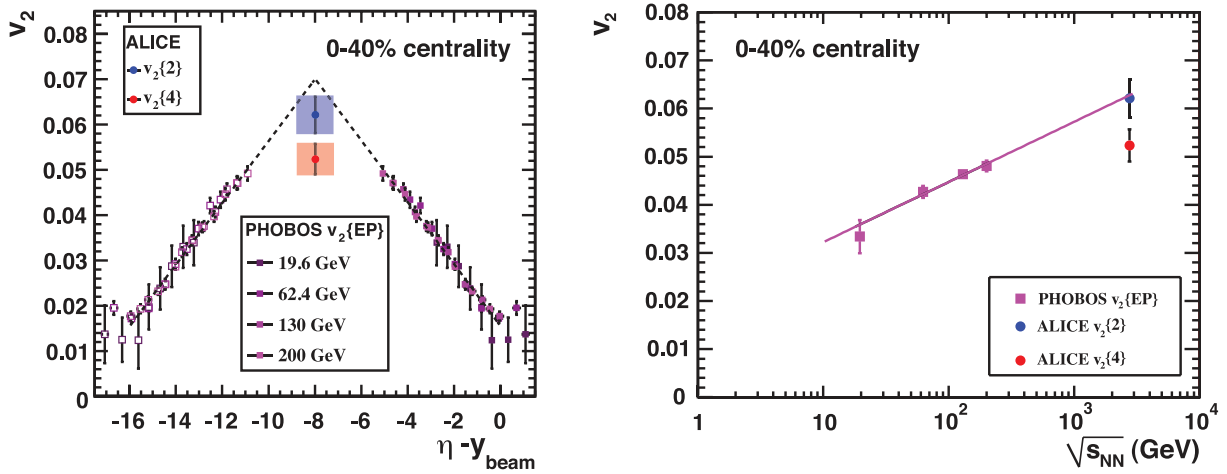
Figure 15. (a) Elliptic flow plotted versus $\eta - y_{\text{beam}}$ for RHIC and LHC, where for y_{beam} the $\sqrt{s_{\text{NN}}} = 2.76\,\text{GeV}$ value is used. The mesh shows the η-range over which the elliptic flow is constant within statistical uncertainties. (b) Elliptic flow versus beam energy. In both figures, the uncertainties of ALICE are systematic uncertainties and the v_2 in 0–40% centrality is obtained by averaging over events instead of over the more commonly used particle yield.

Figure 15(b) shows that the energy dependence of elliptic flow at midrapidity also seems to follow a rather simple scaling: the measured elliptic flow for four beam energies at RHIC shows a linear increase; extrapolating this to $\sqrt{s_{\text{NN}}} = 2.76\,\text{TeV}$ results in a v_2 that agrees well with the ALICE measurement.

The observed increase in the elliptic flow as a function of beam energy is due either to an increase in p_t-differential flow or to an increase in the average transverse momentum of the charged particles. In most hydrodynamic model calculations, the p_t-differential elliptic flow of charged particles does not change significantly [51, 52], while the radial (azimuthally symmetric) flow does increase, which leads to an increase in the average transverse momentum. The larger radial flow also leads to a decrease in the elliptic flow at low transverse momentum, which is most pronounced for heavy particles. Figure 16(a) compares the p_t-differential elliptic flow of charged particles for three centralities at the LHC with STAR measurements at RHIC. It is seen that the p_t-differential elliptic flow is the same within experimental uncertainties. In figure 16(b), the p_t-differential elliptic flow measured at four beam energies is shown. The agreement of $v_2(p_t)$ at these beam energies, which differ by almost two orders of magnitude, is remarkable. Measurements of identified particle elliptic flow at these energies will reveal whether this agreement can be understood in hydrodynamic model calculations.

6. Summary

In this review, I have shown that elliptic flow is one of the most informative observables in heavy-ion collisions. Nevertheless, the wealth of experimental information obtained from elliptic flow is far from being fully explored. The theoretical understanding of the experimental data is rapidly improving, as is our understanding of the dynamics of heavy-ion collisions and the properties of the new state of matter, the QGP. New high-quality data from the LHC
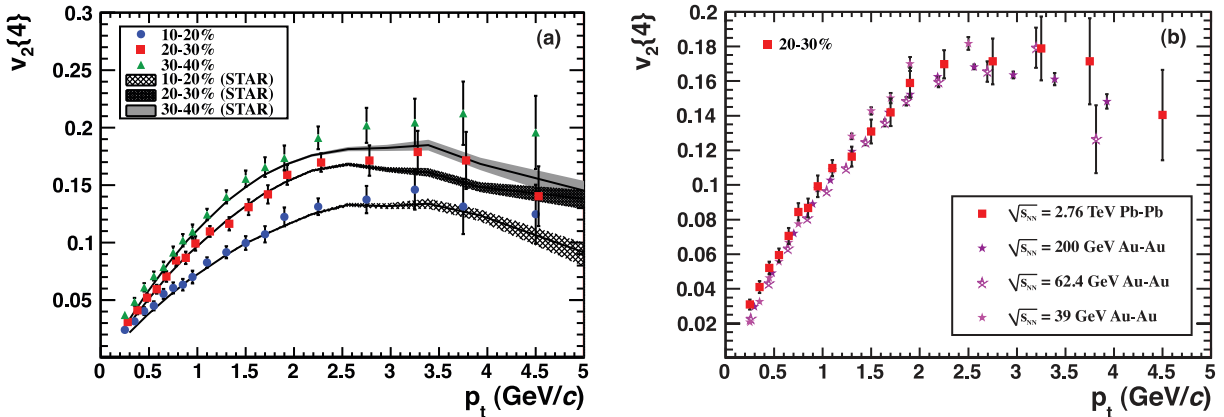
IOP Institute of Physics ✿ DEUTSCHE PHYSIKALISCHE GESELLSCHAFT

Figure 16. (a) $v_2\{4\}(p_t)$ for various centralities compared with STAR measurements. The data points in the 20–30% centrality bin are shifted in p_t for visibility. (b) $v_2\{4\}(p_t)$ for a collision energy range that covers almost two orders of magnitude [60].

recently became available that show that at LHC energies, elliptic flow can be studied with unprecedented precision. This is because of the increase in particle multiplicity and also because of the increase in the flow signal itself. Due to the expected longer lifetime of the QGP and the smaller contributions from the hadronic phase, it is argued that the LHC is also more suitable for determining η/s of the partonic fluid [61]. Measurements of the identified particle elliptic flow at the LHC and in particular the stronger mass dependence (splitting) of $v_2(p_t)$ will be important to confirm the current theoretical picture. Additional constraints on η/s can be obtained by measurements of the other anisotropic flow harmonics, v_3, v_4 and v_5. In the near future, these measurements will become available and significantly increase our understanding of ultrarelativistic nuclear collisions and multi-particle production in general.

Acknowledgments

References

 [1] Higgs P W 1964 *Phys. Lett.* **12** 132–3
 [2] Higgs P W 1964 *Phys. Rev. Lett.* **13** 508–9
 [3] Englert F and Brout R 1964 *Phys. Rev. Lett.* **13** 321–2
 [4] Nambu Y and Jona-Lasinio G 1961 *Phys. Rev.* **122** 345–58
 [5] Gross D J and Wilczek F 1973 *Phys. Rev.* D **8** 3633–52
 [6] Politzer D H 1973 *Phys. Rev. Lett.* **30** 1346–9
 [7] Shuryak E V 1980 *Phys. Rep.* **61** 71–158
 [8] Bazavov A *et al* 2009 *Phys. Rev.* D **80** 014504
 [9] Chapline G F, Johnson M H, Teller E and Weiss M S 1973 *Phys. Rev.* D **8** 4302–8
[10] Lee T D and Wick G C 1974 *Phys. Rev.* D **9** 2291

[11] Lee T D 1979 *Phys. Rev.* D **19** 1802
[12] Collins J C and Perry M J 1975 *Phys. Rev. Lett.* **34** 1353
[13] Pisarski R D and Wilczek F 1984 *Phys. Rev.* D **29** 338–41
[14] Ollitrault J Y 1992 *Phys. Rev.* D **46** 229
[15] Voloshin S A, Poskanzer A M and Snellings R 2010 *Relativistic Heavy Ion Physics* vol 1/23 (Berlin: Springer) pp 5–54 (arXiv:0809.2949 [nucl-ex])
[16] Heinz U W 2009 arXiv:0901.4355 [nucl-th]
[17] Huovinen P and Ruuskanen P V 2006 *Annu. Rev. Nucl. Part. Sci.* **56** 163
[18] Teaney D A 2009 arXiv:0905.2433 [nucl-th]
[19] Miller M L *et al* 2007 *Annu. Rev. Nucl. Part. Sci.* **57** 205–43
[20] Aamodt K *et al* (ALICE Collaboration) 2010 *Phys. Rev. Lett.* **105** 252302
[21] Kolb P F and Heinz U W 2004 *Quark Gluon Plasma* ed R C Hwa *et al* (Singapore: World Scientific) pp 634–714
[22] Huovinen P and Petreczky P 2010 *Nucl. Phys.* A **837** 26–53
[23] Teaney D 2003 *Phys. Rev.* C **68** 034913
[24] Luzum M and Romatschke P 2008 *Phys. Rev.* C **78** 034915
[25] Kovtun P, Son D T and Starinets A O 2005 *Phys. Rev. Lett.* **94** 111601
[26] Csernai L P, Kapusta J I and McLerran L D 2006 *Phys. Rev. Lett.* **97** 152303
[27] Lacey R A *et al* 2007 *Phys. Rev. Lett.* **98** 092301
[28] Hirano T *et al* 2007 *J. Phys. G: Nucl. Part. Phys.* **34** S879–82
[29] Borghini N, Dinh P M and Ollitrault J-Y 2001 *Phys. Rev.* C **64** 054901
[30] Adler C *et al* (STAR Collaboration) 2002 *Phys. Rev.* C **66** 034904
[31] Bilandzic A, Snellings R and Voloshin S 2011 *Phys. Rev.* C **83** 044913
[32] Miller M and Snellings R 2003 arXiv:nucl-ex/0312008
[33] Manly S *et al* (PHOBOS Collaboration) 2006 *Nucl. Phys.* A **774** 523
[34] Sorensen P 2009 arXiv:0905.0174 [nucl-ex]
[35] Qin G-Y *et al* 2010 *Phys. Rev.* C **82** 064903
[36] Lacey R A *et al* 2010 arXiv:1009.5230 [nucl-ex]
[37] Hirano T and Nara Y 2009 *Nucl. Phys.* A **830** 191C–4C
[38] Ollitrault J-Y, Poskanzer A M and Voloshin S A 2009 *Phys. Rev.* C **80** 014904
[39] Mrowczynski S 2009 *Acta Phys. Pol.* B **40** 1053–74
[40] Bhalerao R S and Ollitrault J-Y 2006 *Phys. Lett.* B **641** 260–4
[41] Voloshin S A *et al* 2008 *Phys. Lett.* B **659** 537–41
[42] Alver B *et al* 2008 *Phys. Rev.* C **77** 014906
[43] Lin Z-W *et al* 2005 *Phys. Rev.* C **72** 064901
[44] Arsene I *et al* 2005 *Nucl. Phys.* A **757** 1
     Back B B *et al* 2005 *Nucl. Phys.* A **757** 28
     Adams J *et al* 2005 *Nucl. Phys.* A **757** 102
     Adcox K *et al* 2005 *Nucl. Phys.* A **757** 184
[45] Gyulassy M and McLerran L 2005 *Nucl. Phys.* A **750** 30
[46] Shen C *et al* 2010 *Phys. Rev.* C **82** 054904
[47] Song H *et al* 2010 arXiv:1011.2783 [nucl-th]
[48] Masui H *et al* 2009 *Nucl. Phys.* A **830** 463C–6C
[49] Nagle J L, Steinberg P and Zajc W A 2010 *Phys. Rev.* C **81** 024901
[50] Song H *et al* 2011 arXiv:1101.4638 [nucl-th]
[51] Niemi H, Eskola K J and Ruuskanen P V 2009 *Phys. Rev.* C **79** 024903
[52] Kestin G and Heinz U W 2009 *Eur. Phys. J.* C **61** 545
[53] Luzum M and Romatschke P 2009 *Phys. Rev. Lett.* **103** 262302
[54] Hirano T, Huovinen P and Nara Y 2010 arXiv:1010.6222 [nucl-th]

[55] Hirano T, Heinz U W, Kharzeev D, Lacey R and Nara Y 2006 *Phys. Lett.* B **636** 299

[56] Luzum M 2010 arXiv:1011.5173 [nucl-th]

[57] Heinz U and Shen C 2010 private communication

[58] Back B B *et al* (PHOBOS Collaboration) 2005 *Phys. Rev. Lett.* **94** 122303

[59] Busza W 2008 *J. Phys. G: Nucl. Part. Phys.* **35** 044040

[60] Kumar L (FTS Collaboration) 2011 arXiv:1101.4310 [nucl-ex]

[61] Niemi H *et al* 2011 arXiv:1101.2442 [nucl-th]